Pseudo Two-Dimensional Modeling of Sediment Build-Up in Centrifuges: A Compartment Approach Using Compressional Rheology

Lars E. Spelter and Hermann Nirschl
Institute for Mechanical Process Engineering and Mechanics, Karlsruhe Institute of Technology, Campus Sued, Strasse am Forum 8, 76131 Karlsruhe, Germany

Anthony D. Stickland and Peter J. Scales
Particulate Fluids Processing Centre, Dept. of Chemical and Biomolecular Engineering, The University of Melbourne, Parkville, Australia

DOI 10.1002/aic.14115
Published online May 1, 2013 in Wiley Online Library (wileyonlinelibrary.com)

Both a new modeling approach and new experimental data for the sediment build-up in centrifuges are presented. In semibatch apparatus, the suspension is continuously fed to the centrifuge, separating the particles inside the rotor and discharging the clarified liquid. The solid phase is removed once the capacity of the centrifuge is reached. The solids fraction of the sediment depends on the rheological properties of the cake. The sediment growth and consolidation throughout the process can be calculated using a pseudo two-dimensional approach that takes into account particle-size dependent settling, sediment compressibility, the centrifugal force field, and the geometry of the bowl. The predictions of the separation behavior and the particle-size distributions of the sediment and overflow are compared with experimentally obtained results, showing improved accuracy when compared to simpler models. The model presented is applicable to all solid-bowl centrifuges without conveying systems. © 2013 American Institute of Chemical Engineers *AIChE J*, 59: 3843–3855, 2013

Keywords: design (process simulation), fluid mechanics, rheology, settling/sedimentation, solid–liquid separations

Introduction

The separation of particulates that are dispersed in a continuous phase is an important unit operation in various industrial processes. Centrifuges are found in the minerals,[1] food processing,[2] and pharmaceutical industries.[3] There are two basic principles: continuous and batch centrifugation. While in continuous apparatus, such as decanting centrifuges both the solid and liquid phases are processed continuously, in batch centrifuges the solids accumulate at the wall of the rotor and have to be removed when then solids capacity is reached. In semibatch centrifuges, such as tubular-bowl centrifuges, the solids accumulate at the rotor wall and suspension is fed continuously. The clarified liquid leaves the centrifuge during the batch via an overflow weir. The sediment build-up has a significant influence on the process outcome during the semibatch, because the residence time is reduced by the accumulating solids.[4] It is important to capture the real sediment build-up, because the flow pattern is influenced by the sediment growth. Depending on whether the sediment is plug shaped or homogeneously distributed over the rotor, the interaction between settled solids and flow will be different.

For incompressible products, where the concentration is independent of pressure, the process efficiency can be calculated using an approach developed by Stahl et al.[5] A good agreement was reported for high separation efficiency and coarse products. The model is based on the assumption that all particles coarser than the cut size are separated in the centrifuge and settle close behind the inlet. Thus, a plug-shaped sediment is formed. A distribution of the particles in the flow and slumping and consolidating of the sediment in the axial and radial directions are not considered. Their experimental observations and further investigations by the authors determined a conical shape of the sediment rather than a plug-shaped one.[4,5] The differences between the modeled and observed sediment build-up are caused by the varying settling path of particles with different sizes and different initial radial positions in the flow. The sediment angle decreases with lower separation efficiency, because the particles settle along the entire length of the rotor.[4] If the cut size of the centrifuge exceeds the mean particle size of the dispersed solids, the sediment angle tends to be less than 10°. These effects are not captured by the previously published model by Stahl et al. and the error of the existing model increases significantly due to the disagreement between assumed and observed sediment profile. In later

Correspondence concerning this article should be addressed to L. E. Spelter at lars.spelter@kit.edu.

© 2013 American Institute of Chemical Engineers

versions of the model, a sediment angle was implemented in the calculations, which improved the accuracy, but the angle has to be determined experimentally by photographs or magnetic resonance imaging (MRI). The effort to gain reliable data for the sediment angle is extensive.

A new approach that requires only material functions that can be obtained by well-established experiments may lead to a generally applicable simulation model. The distribution of the particles in the flow as well as the individual settling path of each particle size has to be taken into account. The new theory presented also includes the approach of Buscall and White[6] and Landman and White[7] to describe the consolidation of the cake or sediment due to a compressional load. This approach has been used previously for the one-dimensional (1-D) calculation of the consolidation of various cakes under the influence of the gravitational field of the earth[8] and centrifugal acceleration.[9–12]

Theory

The sediment build-up is calculated by determining the settling path of the particles entering the centrifuge. The particles are homogeneously distributed over the cross-section of the inlet, which exhibits an axial flow velocity. The particles are dragged with the flow toward the outlet and settle in the radial direction toward the bowl wall. Unhindered settling of the particles and negligible yielding or slumping of the formed sediment in the axial direction are assumed. The separated particles are allocated to different compartments, depending on the axial component of the settling path, as depicted in Figure 1. Each compartment accounts for 2% of the overall length of the rotor. The settling paths of two particles of different size are illustrated below the centrifuge axis. According to their different settling paths, the particles are allocated to a different compartment with the width Δl.

By integrating the sediment volume for the time of the semibatch process, the transient sediment build-up is calculated. By knowing the distribution of the solids, it is possible to predict the interaction of the sediment with the flow pattern. Furthermore, the consolidation of the settled particles is determined by compressional rheology using a 1-D approach on each compartment. The scheme of the model is explained in the following section, beginning with the determination of the distribution of the particles in the centrifuge, followed by the compressional model and the application of the 1-D approach on the two-dimensional case. The model proposed is applicable to solid-bowl centrifuges without internal conveying systems, because the fluid motion in conveying centrifuges requires a three-dimensional (3-D) approach.

Two-dimensional model

Two subsequent steps are taken in each time interval Δt. At first, the distribution of the solids throughout the rotor is determined. In a subsequent step, the consolidation of the sediment is calculated. For the prediction of the consolidation, a transient or equilibrium solution may be used.

Determination of the Distribution of the Solids. The basis for the calculation of the settling of the solids in the rotor of the centrifuge is the Stokesian settling velocity w, Eq. 1. The sedimentation velocity of a spherical particle of diameter x depends on the density difference $\Delta\rho$ between the solids and the liquid, the viscosity of the liquid η, the radial position r in respect to the rotational axis, and the rotational speed n.

$$w = \frac{\Delta\rho \cdot x^2 \cdot \left(\frac{2\cdot\pi\cdot n}{60}\right)^2 \cdot r}{18 \cdot \eta} \tag{1}$$

Eq. 1 is applicable for the unhindered settling of a single particle and a laminar flow around the particle. The particle Reynolds number has been calculated in a previous work

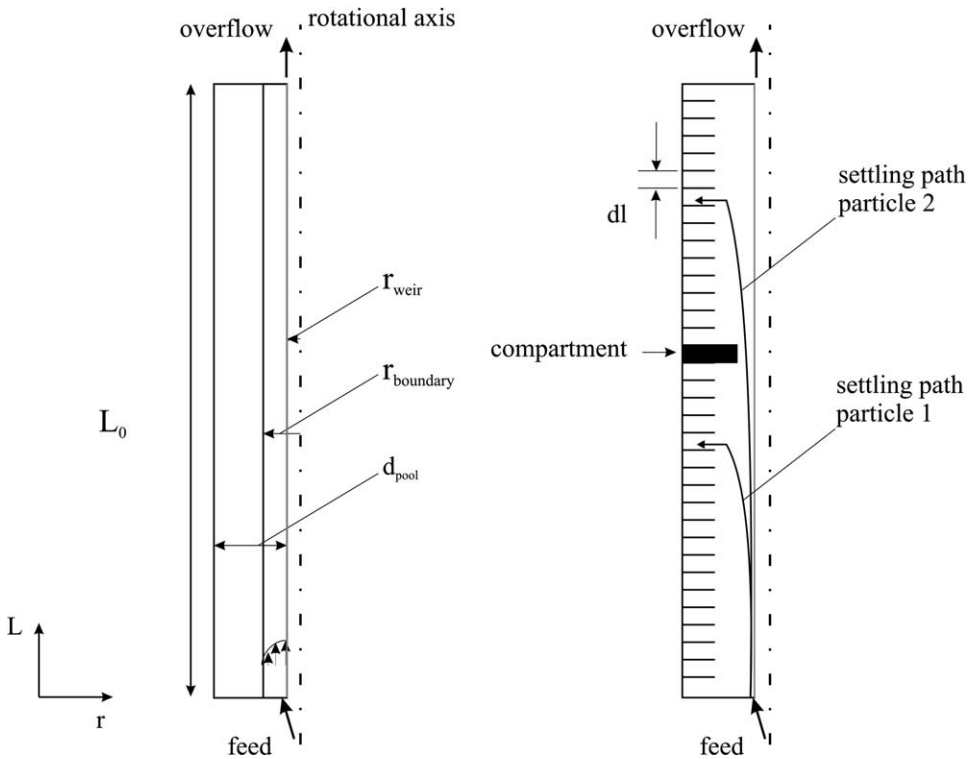

Figure 1. Flow pattern in solid-bowl centrifuges with overflow weir.

showing that the Stokesian approach is applicable to the particle-systems and operating parameters used here.[4] With increasing solids concentration, the settling velocity decreases due to the reduced free cross-sectional area. Whilst dilute suspensions with unhindered settling are used here, hindered settling can be implemented if necessary.[13,14]

The settling of the particles in a centrifuge with a rotor length of L_0 first takes place in a boundary layer flow, where there is strong axial flow. Once the particles have passed this layer, they enter a region in which the axial velocity is one or more orders of magnitude less than in the boundary layer. Therefore, this region is considered as a stagnant pool. A scheme explaining the flow pattern is shown in Figure 1.

The formation of boundary layer flow in centrifugation has been confirmed in solid-bowl,[15,16] low-speed,[17,18] and high-speed tubular bowl centrifuges,[4] and is widely accepted in the solid–liquid separations community.[19,20] The relative width of the boundary layer W is the ratio between layer width d_{flow} ($r_{\text{boundary}} - r_{\text{weir}}$) and pool depth d_{pool}

$$W = \frac{d_{\text{flow}}}{d_{\text{pool}}} \tag{2}$$

and depends on the rotational speed, the viscosity of the liquid and the geometry of the feed system. The boundary layer width must be determined from measurement or fluid dynamics modeling. Considering this flow pattern, Eq. 1 is integrated from the radius of the pool surface r_{weir} to the radius of the boundary layer flow r_{boundary}, Eq. 3.

$$\frac{dr}{dt} = \frac{\Delta\rho \cdot x^2 \cdot \left(\frac{2\cdot\pi\cdot n}{60}\right)^2 \cdot r}{18 \cdot \eta} \Rightarrow \int_{r_{\text{weir}}}^{r_{\text{boundary}}} \frac{1}{r}\, dr = \int_0^t \frac{\Delta\rho \cdot x^2 \cdot \left(\frac{2\cdot\pi\cdot n}{60}\right)^2}{18 \cdot \eta}\, dt \tag{3}$$

The resulting expression of the integration of the Stokesian settling velocity over the width of the boundary layer flow can be rearranged to obtain the settling time t

$$\ln\left(\frac{r_{\text{boundary}}}{r_{\text{weir}}}\right) = \frac{\Delta\rho \cdot x^2 \cdot \left(\frac{2\cdot\pi\cdot n}{60}\right)^2}{18 \cdot \eta} \cdot t \Rightarrow t = \frac{\ln\left(\frac{r_{\text{boundary}}}{r_{\text{weir}}}\right) \cdot 18 \cdot \eta}{\Delta\rho \cdot x^2 \cdot \left(\frac{2\cdot\pi\cdot n}{60}\right)^2} \tag{4}$$

With the settling time, the axial component L of the settling path can be determined by equating the residence time τ

with the settling time $$\tau = \frac{V}{\dot{V}} = \frac{L}{v} \tag{5}$$

$$\begin{aligned} \tau = t \Rightarrow \frac{L}{v} &= \frac{\ln\left(\frac{r_{\text{boundary}}}{r_{\text{weir}}}\right) \cdot 18 \cdot \eta}{\Delta\rho \cdot x^2 \cdot \left(\frac{2\cdot\pi\cdot n}{60}\right)^2} \\ \Rightarrow L &= \frac{\ln\left(\frac{r_{\text{boundary}}}{r_{\text{weir}}}\right) \cdot 18 \cdot \eta \cdot v}{\Delta\rho \cdot x^2 \cdot \left(\frac{2\cdot\pi\cdot n}{60}\right)^2} \end{aligned} \tag{6}$$

The residence time depends on the throughput $\dot{V}$ and the capacity of the centrifuge V. The throughput can be substituted by the axial fluid velocity v in the boundary layer and the cross-sectional area and the volume by the same cross-sectional area and the length. This leads to the right side of Eq. 5. The axial velocity of the particle is determined by the flow profile in the centrifuge. As mentioned before, a boundary layer flow was observed in this type of centrifuge. Measurements of the residence time yielded a change in flow pattern with increasing fill level.[21] The initial width of the boundary layer when there is no sediment (i.e., at a fill level of 0%) decreases after most of the cross-section is blocked by the sediment (see Figure 20). A blockage close to the inlet is sufficient to change the overall width throughout the remaining length of the rotor. Hence, the flow profile is calculated with respect to the fill level. With increasing fill level, the width of the boundary layer flow is reduced till the minimum thickness is reached, which was between 2 and 30 mm (14–32% of the pool depth) depending on the type of centrifuge and the operational parameters.

The axial component of the settling path has to be calculated for each particle size occurring in the suspension. By doing so, the distribution of solids in the cylinder is accessible. The sum size distribution $Q_3(x)$ determines the amount of solids in each interval Δx. By applying Eq. 7, the volume of solids with the particle size x is calculated and deposited at the determined axial position. It depends on the volume flux, the solids fraction of the feed c_{V} and the time interval Δt.

$$V = \dot{V} \cdot c_v \cdot \Delta t \tag{7}$$

The flow profile as a function of the radial position at the inlet is taken into account by dividing the boundary layer in k slices. Instead of using a constant flow velocity as depicted in Figure 2a, each slice with the width s may have a different flow velocity, as shown in Figure 2b. With the discretized width of the flow, it is possible to model either a distribution of solids close to the liquid–gas interface as shown in Figure 2c or a homogeneous distribution of the solids over all slices as depicted in Figure 2d. As the practical case will be a combination of the cases b and d, for the simulations presented the volume of solids V that enters the centrifuge is distributed over all slices that exhibit different axial flow velocities, as shown in Figure 2e. With a constant slice thickness, the area of each slice increases due to the cylindrical shape. The distribution of the solids is weighted by the increase of area so that the solids concentration in each layer is constant

$$V_j = \frac{A_{\text{ki}}}{A_{\text{boundaryflow}}} \cdot V \tag{8}$$

with

$$A_{\text{boundary flow}} = \pi \cdot \left(r_{\text{boundary}}^2 - r_{\text{weir}}^2\right) \tag{9}$$

The axial component L of the settling path is then calculated for all particle sizes in each layer subsequently. The result of these calculations is the vector of the axial component of the settling path and the volume of solids for each particle size for each slice. The radial distribution of particles at the inlet of the centrifuge and the calculation of the settling path of all particles beginning from different positions is contrary to most models that describe the settling path of a particle in a centrifuge.[22–24] The proposed slice approach is able to describe the experimentally observed effect that, for a separation efficiency of 50%, the particle-size distributions of the sediment and the feed are similar, whereas the overflow contains essentially just fine particles.[5,25] The presence of significant fractions of fine particulates in the sediment is explainable by the distribution of

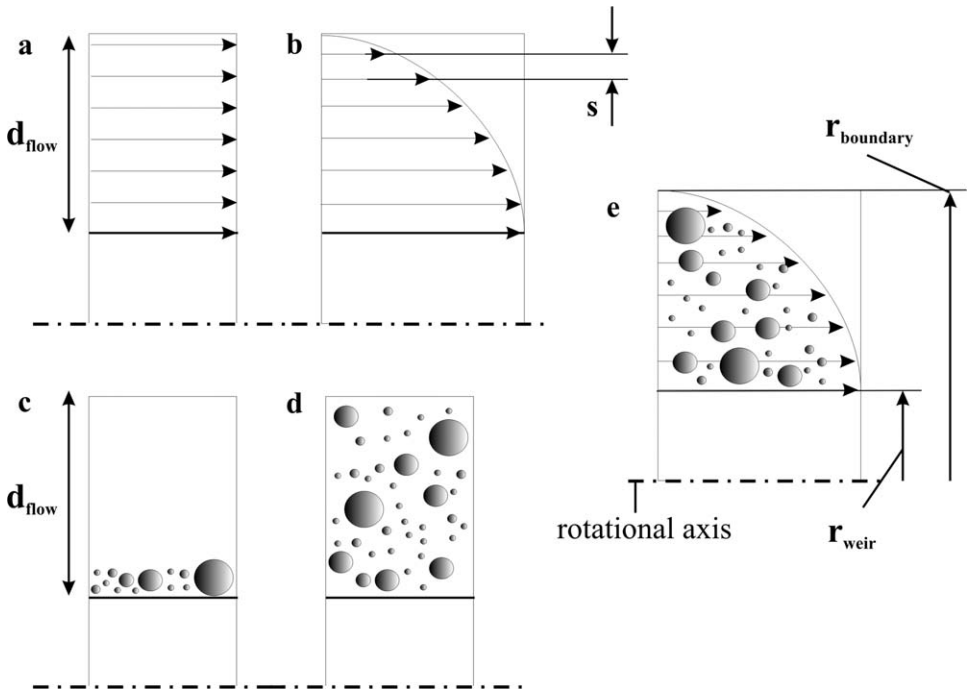

Figure 2. Distribution of the solids in the flow.

(a) plug flow profile, (b) parabolic flow profile, (c) distribution of solids close to rotational axis, (d) distribution throughout boundary layer, and (e) combination of flow profile and distribution of solids as proposed by the authors.

the solids over the cross-sectional area of the boundary layer flow. For example, a fine particle entering the centrifuge close to the interface between boundary layer flow and stagnant sublayer will quickly enter the stagnant pool and settle to the wall, whereas a fine particle entering at the interface between gas and liquid will travel further. Therefore, the particle-size distribution of the sediment exhibits no considerable segregation in axial and radial coordinate. This is disadvantageous for classification tasks. If a narrow particle-size distribution of the classified product is desired, the process parameters will need adjustment so that only the fine particulates close to the interface between gas and liquid are discharged via the overflow weir. By doing so, the overflow fraction will exhibit a narrow particle-size distribution, as confirmed experimentally.[25]

Some authors explained the occurrence of fine particles in the coarse fraction by the fish-hook effect,[26,27] which, to the opinion of the authors, may not be the case, especially in centrifuges. The rarely observed fish-hook effect is a phenomenon that has been observed in small hydrocyclones. The effect is explained by turbulent flow pattern[28] with Re-particle-numbers above 0.5 up to 25. The particle Re-number in centrifuges is significantly higher, because the centrifugal force is created by the rotating liquid and not by the fluid flow as it is the case for hydrocyclones. Hence, the "fish-hook effect" will not occur in centrifuges but may be caused by improper particle-size techniques[29] and the distribution of particles in the flow as mentioned before. Furthermore, the fine particles are underweighted in most particle sizers and the confidence level of the data is low due to the lower particle number.

For small particles in a slice close to the surface of the pool, the calculated axial sedimentation path may exceed the length of the rotor. In this case, these particles are not separated and not further included in the calculation of the sediment build-up in the actual time step. The remaining particles are allocated to a corresponding position l in the centrifuge. With the particle-size distribution of the product, the volume corresponding to each particle size V_x is calculated from

$$V_{j,x\,i} = V_j \cdot (Q_3(xi+1) - Q_3(xi)) \tag{10}$$

By this, the volume of solids in each interval Δl over the entire length L_0 is determined

$$V_{solids} = \sum_{d=1}^{k} V_{j,x\,i} \tag{11}$$

With the distribution of the volume in the rotor the radius of the sediment is calculated with

$$r_{sed} = \sqrt{\frac{r_{bowl}^2 - V_{solids}}{\Delta l \cdot \pi}} \tag{12}$$

Once the radius of the sediment in a section Δl (see Figure 1) is equal to the radius of the boundary layer flow $r_{boundary}$, no further sedimentation of particles is possible. When necessary, the consolidation of the sediment in each compartment is calculated prior to determining the fill level of the compartments. If particles are allocated in the same timestep to compartments that already reached their capacity, they will be conveyed to the subsequent compartment, until all particles are either deposited in a compartment with capacity or are swept out of the centrifuge. The separation efficiency in a specific timestep is thus the mass balance of particles that are swept out of the centrifuge and the particles

in the fed suspension at this very moment (see Figure 15). The separation efficiency for each particle size gives the grade efficiency (see Figure 21).

The timestep necessary for a detailed prediction of the sediment shape depends on the volume flow, material and solids concentration of the feed. It was set to one second, which is sufficient for the suspensions and operational parameters that are analyzed. The length of the full section L_{full} is defined by the distance between inlet and the axial position of the last compartment that reached its maximum capacity. This length is added to the calculated axial component of the settling path in the next timestep

$$L' = L + L_{full} \tag{13}$$

Equation 13 accounts for the experimentally observed decrease of separation efficiency with increasing fill level U, because the residence time decreases with increasing L_{full} acc. to Eq. 5. The cut size increases with lower residence times (see Eq. 6). The fill level U is defined as the relationship between the accumulated solids volume to the capacity of the centrifuge V_{cap}

$$U = \frac{L_{full}}{L_0} = \frac{V_{solids}}{V_{cap}} \tag{14}$$

Consolidation Model. The compressibility of the sediment is taken into account using the compressional rheology approach of Buscall and White.[6] In this approach, the particles in the sediment form a continuous network such that the solid phase is able to transmit stress. The local volume fraction of the particulate network in each compartment is a function of radius and time, $\phi(r, t)$. The network has a compressive strength, $p_y(\phi)$, at concentrations above the gel point, ϕ_g, and will consolidate if the local network stress exceeds $p_y(\phi)$. $p_y(\phi)$ is often described using a power-law function[7] such as

$$p_y(\phi) = p_1 \left[\left(\frac{\phi}{\phi_g} \right)^{p_2} - 1 \right] \tag{15}$$

where p_1 and p_2 are experimentally determined fitting parameters.

The rate of consolidation is determined from the hindered settling function, $R(\phi)$, which accounts for the solid–liquid drag. $R(\phi)$ is the resistance of flow through the network and is inversely proportional to permeability. $R(0)$ is the Stokes drag coefficient at an infinite dilution. As with $p_y(\phi)$, $R(\phi)$ is also commonly given as a power-law function[7]

$$R(\phi) = r_1 (1-\phi)^{r_2} \tag{16}$$

In the approach of Buscall and White,[6] the consolidation of the network is described by the momentum balance of hydrodynamic, hydrostatic, network pressure, and acceleration forces acting on a local volume element of suspension. This approach has been used successfully to model various filtration, sedimentation, and centrifugation applications.

Consolidation in Each Compartment. The consolidation of the accumulated solids is calculated in each compartment at each timestep using the approach of Stickland et al.[9] This is performed in parallel with the particle trajectory calculations described earlier. The initially unconsolidated height of solids in the sediment of each compartment is given by the particle trajectory calculations and is assumed to be at the gel point, thus $\phi_0 = \phi_g$.

All variables are dimensionless based on the geometry of the centrifuge and the operational parameters such as the centrifugal force in order to set the initial time and length steps. The radius is made dimensionless with the radius of the bowl

$$Z = 1 - \frac{r^2}{r_{bowl}^2} \tag{17}$$

where Z is the scaled coordinate. The compressive strength is scaled by the centrifugal acceleration to give $P_y(\phi)$

$$P_y(\phi) = \frac{p_y(\phi)}{p*} = \frac{p_y(\phi)}{\Delta\rho\omega^2 r_{bowl}^2} \tag{18}$$

$R(\phi)$ is scaled with the hindered settling of the initial concentration to give $B(\phi)$

$$B(\phi) = \frac{R(\phi)}{(1-\phi)^2} \frac{(1-\phi_0)^2}{R(\phi_0)} \tag{19}$$

Subsequently, the appropriate scaled time T for the consolidation is

$$T = \frac{2\Delta\rho\omega^2 (1-\phi_0)^2}{R(\phi_0)} t \tag{20}$$

The solids velocity, $u(r, t)$, is scaled to give $\psi(Z, T)$

$$\psi(Z,T) = \frac{R(\phi_0)}{\Delta\rho\omega^2 r_{bowl}^2 (1-\phi_0)^2} r\phi u \tag{21}$$

With these scaling, the governing equations are

$$\frac{\partial\phi}{\partial Z} = -\frac{1}{\Delta(\phi)} \left[\frac{\phi}{B(\phi)} - \frac{\psi}{1-Z} \right] \tag{22}$$

$$\frac{\partial\psi}{\partial Z} = \frac{\partial\phi}{\partial T} \tag{23}$$

where $\Delta(\phi)$ is the scaled solids diffusivity

$$\Delta(\phi) = \frac{dP_y(\phi)}{d\phi} \frac{1}{B(\phi)} \tag{24}$$

The full transient solution within each compartment is given by the numerical solution of Eqs. 20 and 21 from the bowl wall, $\psi(0, T) = 0$, to the top of the sediment, $\phi(Z_{sed}, T) = \phi_g$. See Stickland et al.,[9] for full details of the numerical scheme.

If the consolidation is relatively fast compared to the sedimentation, then there is no need to calculate the full transient solution. The equilibrium solution for the given solids volume can be used instead, saving considerable calculation time. Setting the velocity to 0 in Eq. 22 gives

$$\frac{d\phi}{dZ} = -\phi \frac{d\phi}{dP_y(\phi)} \tag{25}$$

The boundary conditions for this ordinary differential equation are $\phi(0)$ and $\phi(Z_c) = \phi_g$, where $\phi(0)$ is given by the global conservation of mass

$$P_y[\phi(0)] = Z_{sed}\phi_0 \tag{26}$$

Z_{sed} is the initial scaled height of the sediment.

Consolidation in the Compartment Approach. The consolidation of the accumulated solids is calculated in each timestep. When simulating the consolidation in all segments Δl, the computational demand increases linearly. Applying the equilibrium solution of the sediment consolidation reduces the computational costs by >98%. Hence, it is advantageous to compare the transient solution at the time where all solids have settled with the equilibrium profile. If the difference between transient and equilibrium solution is negligible, the equilibrium solution is used.

The consolidated sediment build-up is calculated parallel to the nonconsolidated one. For the calculation of the consolidation in each timestep, the actual height r_{sed} (from Eq. 12) from the unconsolidated sediment is taken as the initial condition. Therefore, provided the equilibrium solution can be used, it is not necessary to take the state of the compressed sediment in the timestep before into account. This reduces the computational demand and the comparison between consolidated and nonconsolidated sediment is possible for each timestep. The fill level is determined via the consolidated sediment height.

Centrifuges and materials

Centrifuges. The sediment build-up is calculated for the separation and screening in a tubular bowl and an industrial solid-bowl centrifuge. The centrifuges are both semibatch apparatuses. The geometries of the different rotors are shown in Figure 3.

The tubular-bowl centrifuge has a solids capacity of 250 mL. The maximum rotational speed of the tubular centrifuge is 40,000 rpm, creating the multiple of the earth gravitational field G of 38,700. The length of the cylindrical section of the rotor measures 175 mm, the inlet section equals 28 mm. The radius of the inner wall of the rotor equals 21.5 mm. The suspension enters the tubular centrifuge via a nozzle through the bottom end of the cylinder, which has a radius of 3.9 mm, and is accelerated via rotating blades, which are 10-mm high. The clarified liquid leaves the centrifuge via an overflow weir that has a radius of 7.3 mm. The turbulent inlet zone in the tubular centrifuge creates a boundary layer flow with a higher relative width than the industrial feeder. The liquid is fed on top of a stabilized rotating pool in the industrial centrifuge that reduces mixing significantly. The four blades in the inlet section of the tubular centrifuge mix the incoming liquid partially with the rotating pool. Once the inlet is blocked with sediment, a profile similar to the one in the industrial centrifuge is developed. The exact profile has been determined by computational fluid dynamics (CFD) simulations[25,30] and measurements of the residence time for different process conditions.

The solids capacity of the industrial centrifuge is 12 kg and, thus, significantly higher than the capacity of the tubular-bowl centrifuge. The industrial apparatus reaches 2550 rpm creating 1780 G at the outer diameter of the rotor. The shape of the rotor changes at a height of 191 mm and a radius of 247 mm. The overall length of the centrifuges rotor equals 364 mm. The maximum inner radius of the rotor is 263 mm. The suspension is fed via a rotating cone 59 mm above the lower end of the rotating liquid. The free jet leaves the feeder at a radius of 117 mm. The liquid is discharged via an overflow weir with a radius of 168 mm.

Experimental results using these two centrifuges are compared with model calculations based on material properties and operating conditions to validate the accuracy of the model and the assumptions of Stokesian settling and rigid behavior of the sediment in an axial direction.

Materials. Four different materials were used in this study. Submicron-sized silica (Aerosil 200, Evonik Industries), Kaolin (Sparky GmbH), and yeast cells (Bäko) exhibit slow settling velocities due to their size and density and are thus difficult to separate in centrifuges. This has been shown in previous studies.[4] These products are used for the comparison of the predicted and measured process characteristics of the tubular-bowl centrifuge. Coarser quartz (SF 800, Quarzwerke GmbH) is used for the validation of the prediction of the separation efficiency of the industrial solid-bowl centrifuge. The cumulative particle-size distributions by mass $Q_3(x)$ of the products are shown in Figure 4. The mean diameter is 108 nm for the Aerosil 200, 2.1 μm for the SF 800, 3.9 μm for the yeast cells, and 1.8 μm for the Kaolin.

Compressive Strength and Hindered Settling Function. The compressive strength $p_y(\phi)$ (so far stated as compressive yield stress) and the hindered settling function $R(\phi)$ were determined using filtration and sedimentation methods.[31]

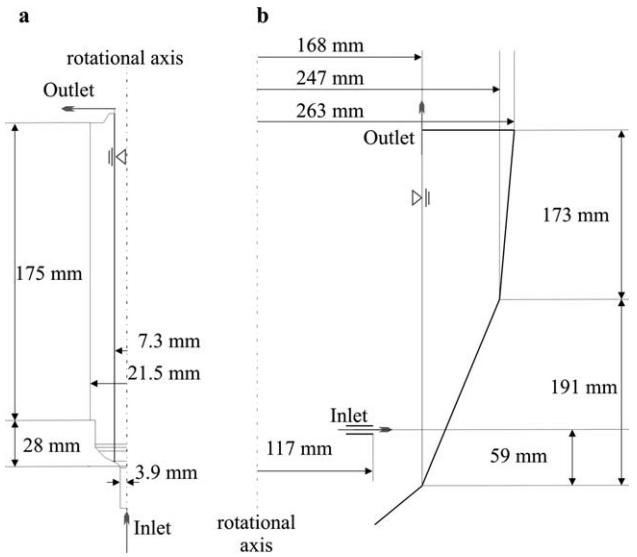

Figure 3. Cross-sectional views.

(a) tubular centrifuge and (b) industrial solid-bowl centrifuge.

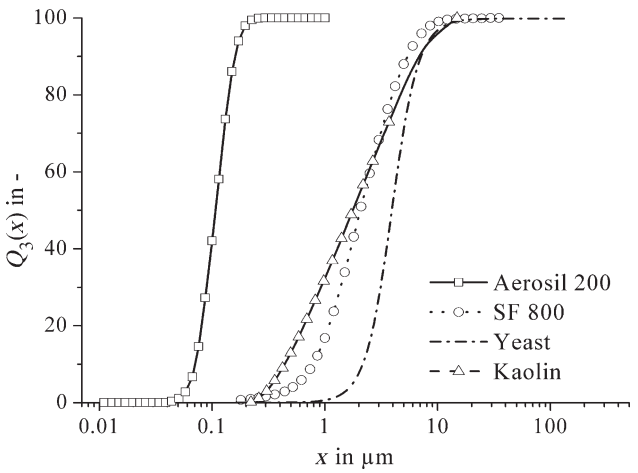

Figure 4. Particle-size distributions of the products used for model validation.

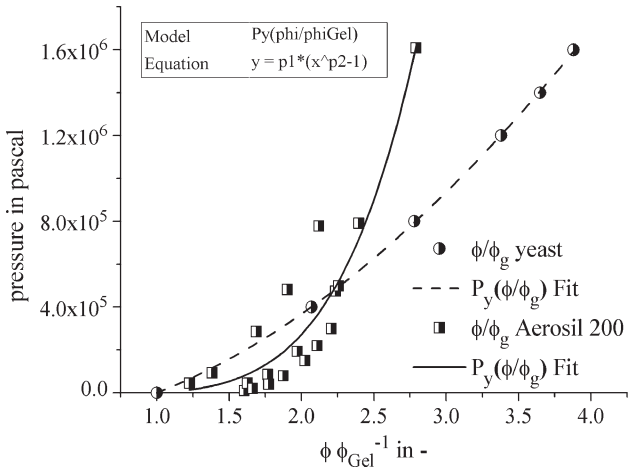

Figure 5. Relationship between applied pressure and solids concentration in sediment.

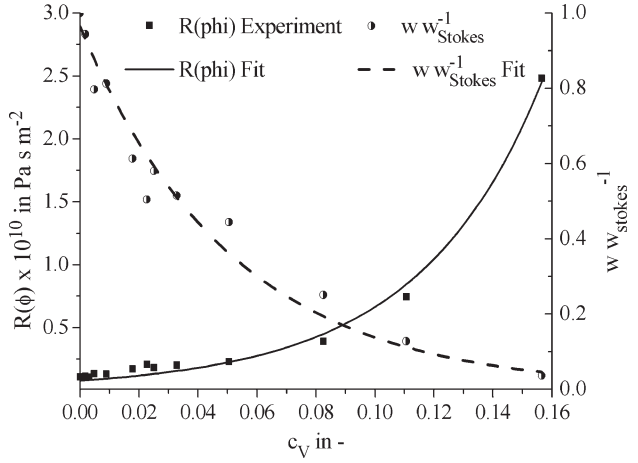

Figure 6. Normalized sedimentation velocity and hindered settling function for yeast cells.

Figure 5 shows the relationship between solids concentration of the sediment and the applied piston pressure for Aerosil 200 and yeast. The experimental data are fitted with Eq. 15 to obtain the parameters p_1 and p_2 of the compressive strength function. The gel point of Aerosil 200 was determined by a rheometer type Haake Mars II[4] and the gel point of the yeast suspension was determined by settling tests.[32]

The experimentally determined parameters of the compressive strength and the parameters of the hindered settling function are given in Table 1.

The hindered settling function characterizes the increase of the resistance that slows down the settling and consolidation process with rising solids volume fraction. Figure 6 shows the experimentally determined settling velocity and the hindered settling function of yeast cells with a mean diameter of 4.1 μm. The settling velocity has been measured in an analytical centrifuge type LUMiFuge and is normalized with the Stokesian settling velocity.

The solids volume fraction of the yeast suspension in the experiments was 0.5 vol %. The influence of the solids volume fraction on the sedimentation velocity is negligible in this regime. Hence, the Richardson–Zaki law is not implemented in the calculation of the sediment build-up. Nevertheless, the hindered settling function increases from 1×10^9 up to 2.5×10^{10} Pa s/m^2 in the examined regime. The parameters r_1 and r_2 are obtained via the curve fit and are implemented in the transient modeling of the sediment compression.

Results and Discussion

Solid-bowl centrifuge

The model is validated by comparing the experimentally determined grade efficiency and grade efficiency curve with the calculated separation behavior of SF 800 Quartz in the industrial solid-bowl centrifuge. In this case, the consolidation of the solids is not taken into account, because the sediment does not grow into the boundary layer and, thus, has no effect on the separation efficiency. The width of the boundary layer flow was determined by CFD and is between 10 and 30 mm. The disturbances of the inlet subside 4 cm after the inlet. This length is considered as a turbulent region and the settling of particles begins after this zone.

Table 1. Parameters of Compressive Strength and Hindered Settling Function

Product	r_1 (Pa s/m^2)	R_2	p_1 (Pa)	P_2
Aerosil 200	5.71×10^{13}	1.17	7222	5.28
Kaolin	8.41×10^{10}	0.67	Incompressible	Incompressible
SF 800	3.44×10^{10}	0.37	Incompressible	Incompressible
Yeast	8.28×10^{8}	−18.89	140,980	1.85

Prediction of the Separation Efficiency. Figure 7 shows the comparison between the calculated and experimentally determined separation efficiency as a function of the volume flux. The experiment at 2550 rpm was repeated thrice to investigate the experimental variability. The data plotted show the mean values and the standard deviation is stated via the error bars. The calculated values slightly overestimate the grade efficiency. The deviation is 16.78% with a standard deviation of 2.68%. The calculated values overestimate the experimental ones most likely, because a fully developed boundary layer flow with an ideal profile within the layer is assumed. The 3-D CFD simulations[30] show that the width of the boundary layer depends on the angle of rotation, because baffles in the centrifuge cause disturbances. Furthermore, the changing efficiency of the acceleration

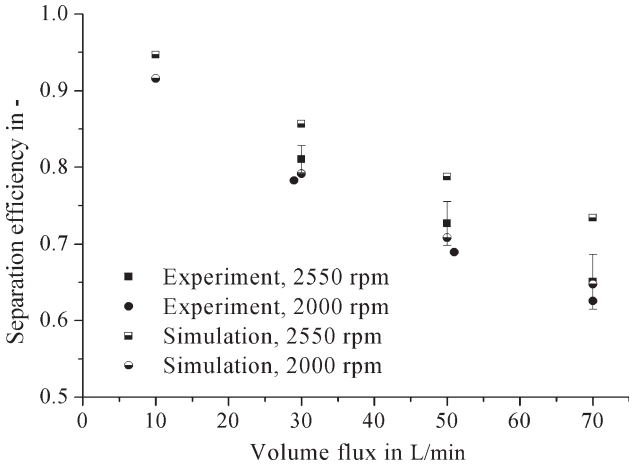

Figure 7. SF 800: Separation efficiency vs. volume flux—comparison of calculated and experimental results; experimental data with permission from Romani.[33]

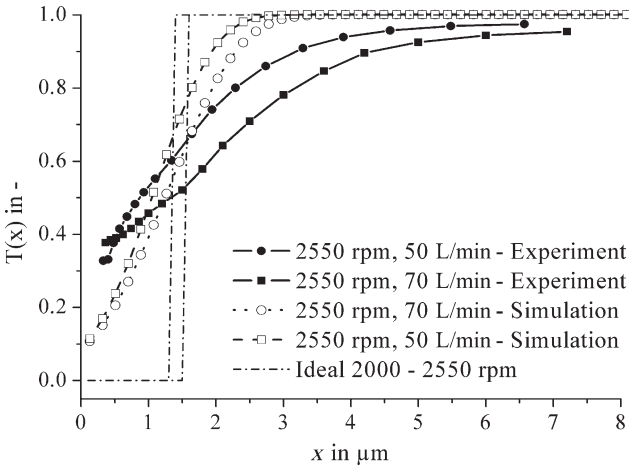

Figure 8. SF 800: Grade efficiency curve for 2550 rpm and two throughputs—comparison of calculated and experimental results; experimental data with permission from Romani.[33]

system of the centrifuge with increasing volume flow and rotational speed causes a lag in tangential velocity of the incoming suspension close to the inlet of the centrifuge. The deviation of the model increases with these parameters.

The cumulative separation efficiency, as shown in Figure 7, is an important result that allows determining whether a product is separated in a centrifuge or discharged via the overflow. The grade efficiency curve $T(x)$ further allows the detailed analysis of the apparatus for classification tasks. The calculated, experimentally determined, and ideal grade efficiency curves for two different throughputs are shown in Figure 8. The ideal curves result from the calculation of the cut size by neglecting the distribution of solids in the boundary layer flow. Taking this distribution into account, the typical, s-shaped grade efficiency curves are obtained. A comparison with the experimentally determined curves show deviations, but a significantly more accurate behavior is determined than in the case for the ideal ones.

Modeling of Several Subsequent Cycles. The solid-bowl centrifuge has a maximum solids load of 12 kg. When this amount is reached, the centrifuge has to be stopped. The batch time can be calculated using the proposed model as shown in Figure 9. The diagram shows four cycles of the

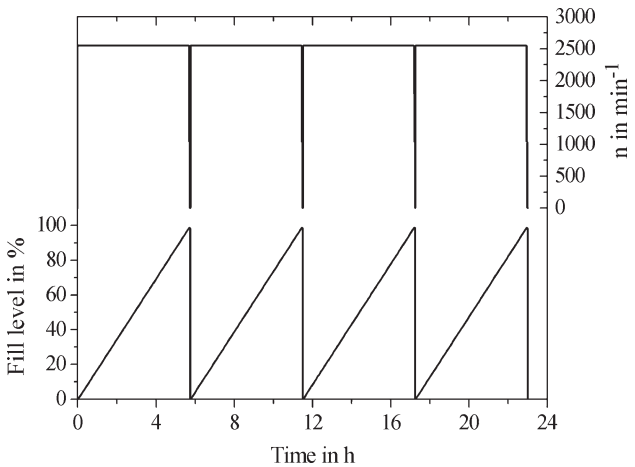

Figure 9. Calculated fill level U (Eq. 14) SF800, 50 L/min throughput, $c_V = 0.02\%$.

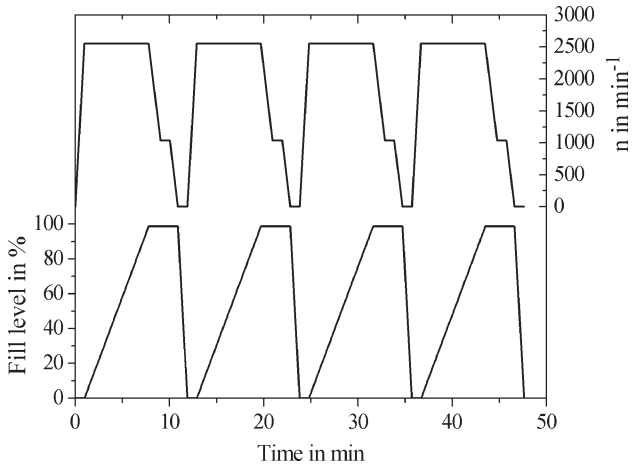

Figure 10. Calculated fill level SF800, 50 L/min throughput, $c_V = 1\%$.

centrifugation process with a solids volume concentration of 0.02% and a constant throughput of 50 L/min, with the corresponding rotational speed plotted on the secondary axis. One cycle consists of bowl acceleration at 2000 rpm/min, start of suspension clarification, stopping of feeding, spin down to 1040 rpm, discharge of the supernatant, spin down to standstill, and discharge of the solids. The duration of the discharge may depends on the material and fill level. For grinding swarf and minerals, the discharge requires approximately 2 min.

While the duration of the centrifugation depends on the solids concentration of the feed, the throughput and the grade efficiency, the spin up and spin down times, supernatant and solids discharge are constant. With increasing solids concentration, the ratio between centrifugation and discharge time decreases. Figure 10 shows the same process as Figure 9 but with a solids volume concentration of the feed of 1%. The cycle time decreases from 5.8 h to 13 min. The model presented here helps to find the appropriate size of the centrifuge to optimize the ratio between process and setup time depending on the properties of the suspension.

Evaluation of the Influence of the Flow Profile on the Separation Efficiency. According to Figure 7, the simulation is in good agreement with the experimental data. For the calculations, a linear flow profile in the boundary layer flow was assumed. Due to the small width of a few millimeters and the high circumferential velocity in the centrifuge, the real profile cannot be measured with hot wire or Laser-Doppler-Anemometers.[34] A comparison of the predicted separation efficiency using different flow profiles in the boundary layer flow with the experimental data is shown in Figure 11. The flow profiles are plotted in the inset of Figure 11. The width of the boundary layer flow was determined by means of CFD.[30,35] For comparing the influence of the flow profile, the width was set constant at a value of 30 mm in all calculations, which are presented in Figure 11.

The flow profile influences the velocity of the particles at a certain radius. While the axial velocity will be constant if a plug flow is assumed, it will decrease linearly or quadratically with the radius in the case of the other flow profiles. However, the overall influence on the grade efficiency is small, so that the assumption of a linear flow profile will cause no significant deviation of the predicted values if compared to the experimental data.

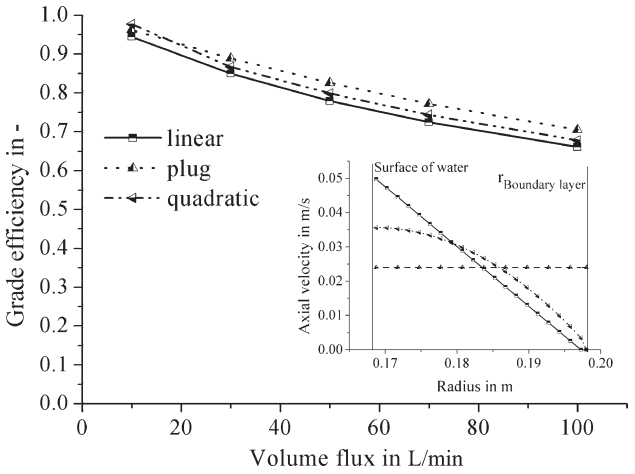

Figure 11. Predicted separation efficiency with different flow profiles in the boundary layer flow and experimental values.

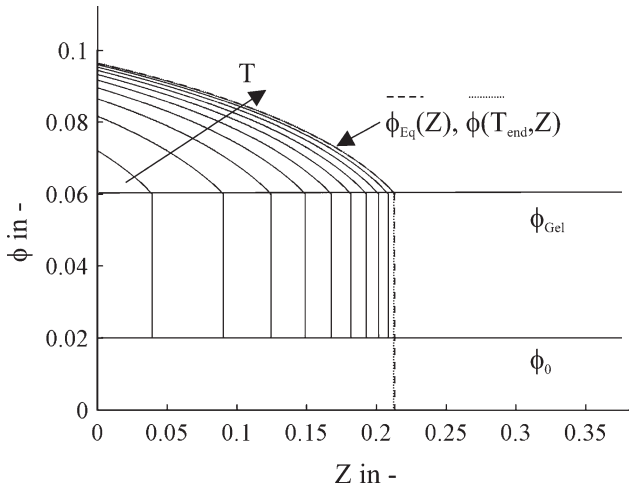

Figure 13. Comparison of equilibrium and time-dependent solution of the consolidation of Aerosil 200 sediment.

Tubular-bowl centrifuge

The separation of fine particulates requires high separation forces. These are achievable with tubular-bowl centrifuges. The following section presents the prediction of the desliming process of a kaolin suspension, the separation of colloidal silica and the settling of yeast cells. Selected computed values are compared with experimental results to validate the methodology.

Desliming of Kaolin. Kaolin is widely used in the paper industry as mineral filler in the coating of the paper. The particles reduce the transmissibility of light. The experience in industrial application is that if the particles are too small, the transmissibility will be too high, due to light transmission through the thin, disc-shaped particles. The aim of the desliming is the reduction of particles below 500 nm. Although not presented here, a comparison of the transmissibility of the paper sheets made of untreated and classified suspension will prove whether the assumption is correct or a different mechanism causes the increased transmissibility.

Figure 12 shows the initial particle-size distribution of the untreated and the deslimed kaolin suspension below 1 μm particle diameter. The overall particle-size distribution is plotted in the upper left corner of the figure. The desliming process was simulated at a rotational speed of 10,500 rpm and a throughput of 1 L/min. The separation efficiency is 50% with these parameters. The simulation predicts a reduction of the fine fraction below 500 nm of 56%. Due to the low separation efficiency and the distribution of the particles in the boundary layer flow (see Figure 2), particles up to 2 μm are dragged out of the centrifuge with the overflow. Nevertheless, the desliming of the fine kaolin suspension with the tubular-bowl centrifuge is successful. This has been validated with experiments.[36] The relative deviation of the predicted and experimentally determined reduction of the fine fraction equals 13.2%.

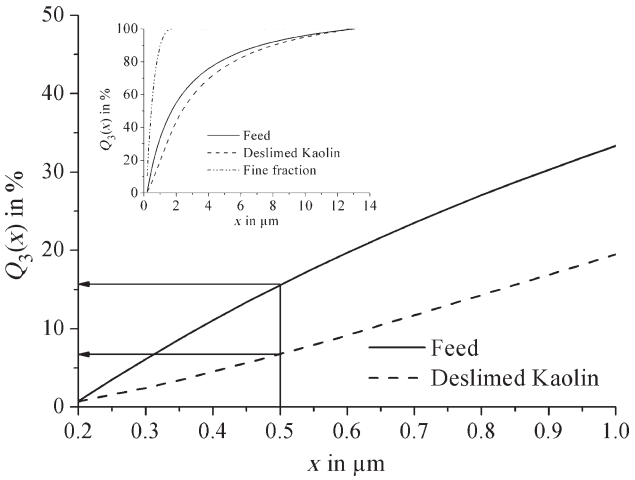

Figure 12. Prediction of the desliming of Kaolin at 10,500 rpm and 1 L/min.

Comparison of the Equilibrium and Time-Dependent Solution. The calculation of the consolidation including the time-dependency of the hindered settling function increases the computational demand significantly. If the rate of bed consolidation is slower than the rate of addition of new solids to the bed (which is dependent on the process conditions and material properties), the time-dependency of the consolidation is negligible and the equilibrium solution can be used. The evaluation is possible by comparing the equilibrium solution of the solids concentration in the sediment ϕ_{eq} with the transient calculation $\phi(T_{end})$. A comparison of these predictions is shown for Aerosil 200 in Figure 13. The solids concentration of the sediment is plotted vs. the dimensionless sediment height. The volume of the solids, which is the area under the lines, increases with time. Due to the increasing weight on the particle network, the sediment consolidates and the solids concentration increases. The last profile plotted is the solids concentration of the sediment at the moment, where all solids have settled and ZS equals zero. If the sediment is not in its equilibrium state, further consolidation takes place and the profile changes until equilibrium is reached. The equilibrium profile matches the transient solution well (the dotted line and the dashed line are overlapping). Hence, the equilibrium state of the cake regarding the solids concentration can be used for the simulation.

Figure 14 shows the height of the sedimentation zone and the growth of the sediment vs. the dimensionless time. The difference between the sediment height at the very moment where all particles have settled (ZS = ZC) compared to the height at equilibrium ZC_∞ is 3.5% and thus negligible.

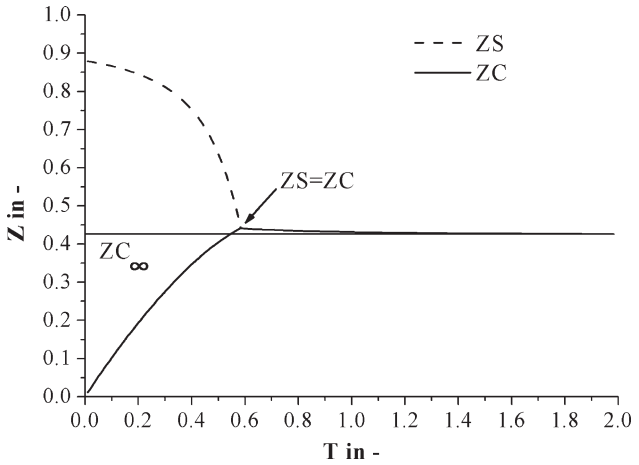

Figure 14. Calculated height of sedimentation zone and sediment consolidation vs. dimensionless time.

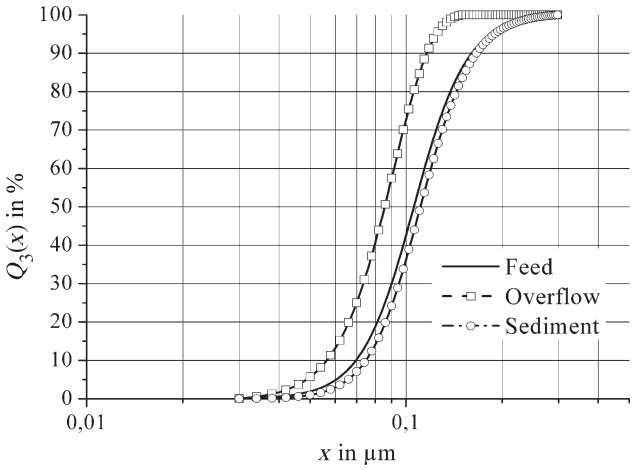

Figure 16. Simulated particle-size distribution for Aerosil 200 of the feed, overflow (fine fraction), and sediment (coarse fraction).

The deviation between the equilibrium and time-dependent solution for the cases presented is small, so that it is acceptable to use the equilibrium solution for modeling the consolidation of the sediments during the semibatch. This reduces the computational time by approximately 98%.

Prediction of the Centrifuge Performance for Aerosil 200 and Yeast. The comparison of the time-dependent and equilibrium solutions yielded a small difference between both approaches such that the equilibrium solution can be used for the calculation. Figure 15 shows the product loss for Aerosil200 for a rotational speed of 40,000 rpm and different throughputs. The comparison between the experimental results with the predictions that takes the compressibility into account (cons.) yields a good agreement. The predictions without the calculation of the sediment consolidation (no cons.) result in an early increase of the product loss. The difference between both models is indicated via the two horizontal arrows.

The predicted product loss is smaller than the experimentally determined one, so that more solids are accumulated in the centrifuge during the same time interval. Hence, the predicted batch time is shorter than observed in the experiments.

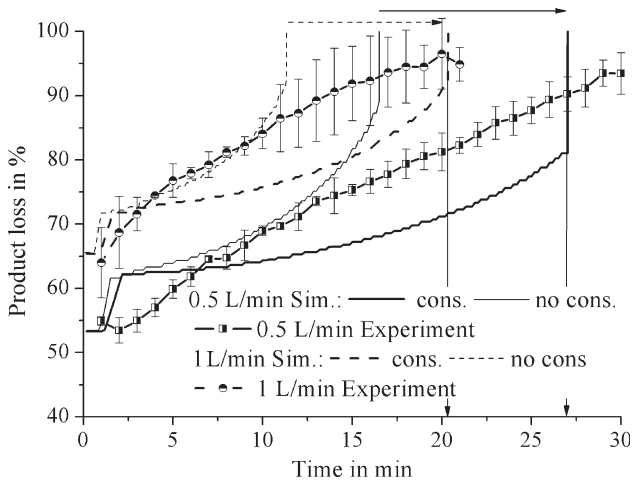

Figure 15. Product loss for Aerosil 200 vs. time—comparison of prediction and experimental results; 40,000 rpm, 0.5 L/min, and 1 L/min.

Nevertheless, the deviation between predicted and true batch time and product loss are small when compared to the overall batch time and product loss. The capacity of the centrifuge is reached earlier when neglecting the consolidation due to the lower solids content of the sediment. Hence, the calculations which take the compressive strength into account increase the accuracy of the prediction of the separation of Aerosil 200.

The advantage of the model presented is the possibility to predict the particle-size distribution of the fine and coarse fraction. These are shown in Figure 16 for Aerosil 200 after calculating the classifying at 40,000 rpm and 0.1 L/min throughput. The product loss is 6% only. Due to the high separation efficiency, only the finest particles are swept out of the centrifuge and, thus, the overflow exhibits a narrow particle-size distribution. Due to the small fraction that is removed from the feed, the particle-size distribution of the sediment is similar to the one of the feed.

The calculated sediment build-up is compared with the experimentally determined build-up in Figure 17 for Aerosil 200 at a rotational speed of 40,000 rpm and a throughput of

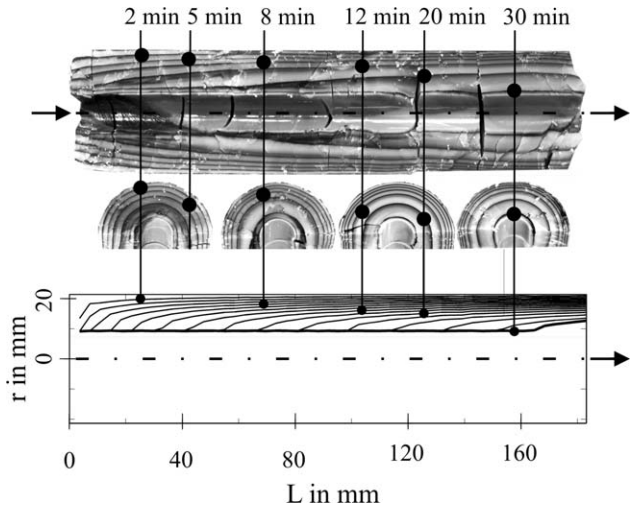

Figure 17. Sediment build-up of Aerosil 200 in the tubular-bowl centrifuge at 40,000 rpm and 0.5 L/min throughput—comparison of prediction (below) and experiment (top).

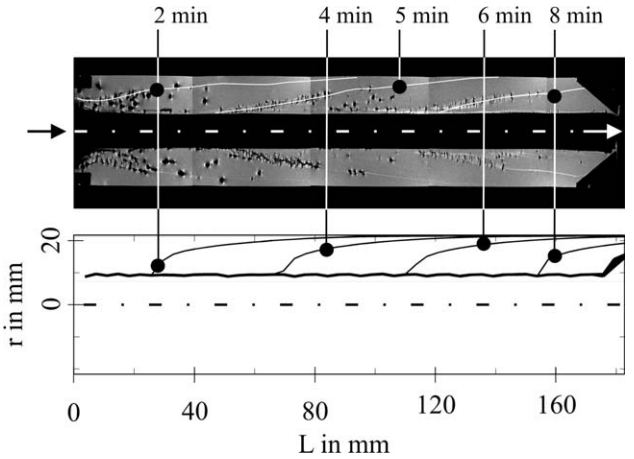

Figure 18. Sediment build-up of yeast cells in the tubular-bowl centrifuge at 20,000 rpm and 1 L/min throughput—comparison of prediction (below) and experiment (top).

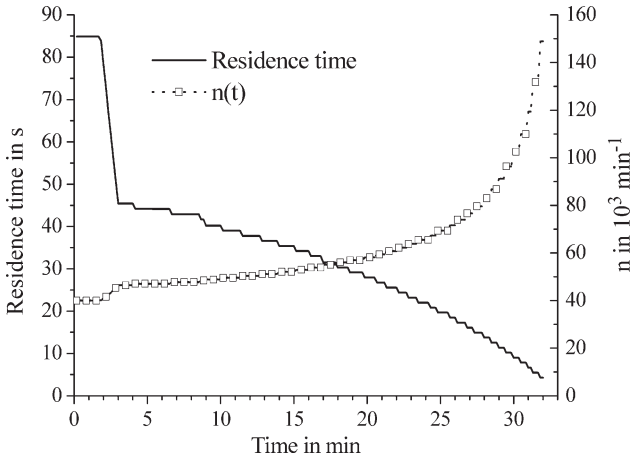

Figure 20. Separation of Aerosil 200; left ordinate: residence time τ (Eq. 5) against time; right ordinate: rotational speed of centrifuge against time.

0.5 L/min. The picture was obtained by halving the sediment and taking a picture with a digital camera. The sediment surface is plotted for every 120 s below the picture. The distribution of solids at a fill level of 98% is highlighted with the thicker line. The sediment build-up exhibits a conical section with a high sediment angle close to the inlet, which is located at the left side, and a conical distribution with a small sediment angle throughout the remaining cylinder. The realistic prediction of the sediment build-up validates the proposed model.

Figure 18 shows a comparison of the experimentally determined sediment build-up of yeast cells with the predicted sediment growth. The upper picture was obtained with MRI. The prediction takes the consolidation of the sediment into account. It agrees well with the real sediment growth.

The product loss of yeast for a constant throughput of 1 L/min and rotational speeds ranging from 10,000 to 40,000 rpm is shown in Figure 19. The results obtained by neglecting the consolidation of the sediment are compared with the simulations using compressional rheology. The product loss decreases with increasing rotational speed. This is due to the increased centrifugal acceleration acting on the settling yeast cells. The steep increase of the product loss curves are caused by the narrow particle-size distribution of the product. At the very moment, where the residence time in the centrifuge is not sufficient to allow the settling of most of the yeast cells, they are swept out of the centrifuge. Due to the sediment build-up, the residence time further decreases. Therefore, the cut size of the centrifuge exceeds the maximum particle size of the cells quickly, causing the sharp increase of the curves. This behavior is not distinctive at 10,000 rpm, because the centrifugal acceleration is not sufficient to capture most of the suspended cells. Hence, the cells settle throughout the length of the rotor, forming an almost homogeneous distributed sediment. Thus, the reduction of the residence time affects the product loss over the entire duration of the batch, but the changes are less pronounced.

The consolidation of the settled yeast cells influences the fill level of the centrifuge. Whilst the compression is almost negligible at 10,000 rpm, the difference in batch time at

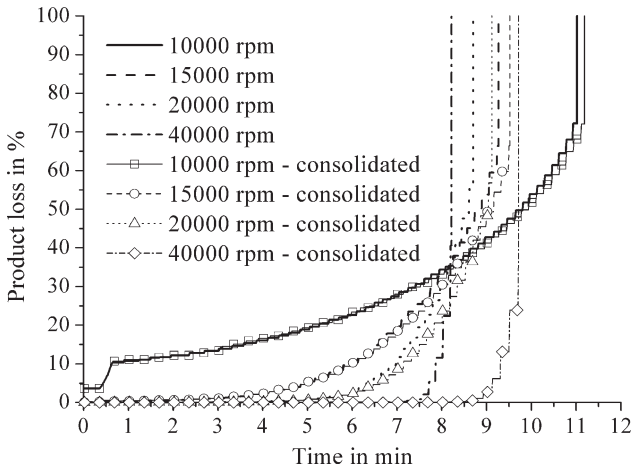

Figure 19. Product loss for yeast cells vs. time—comparison of predictions with and without consolidation.

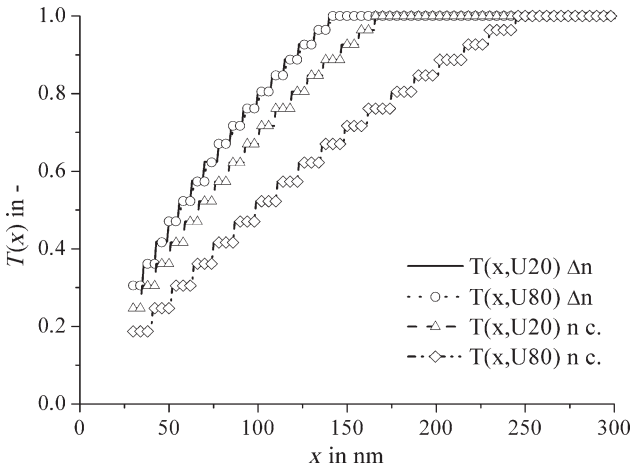

Figure 21. Calculated separation of Aerosil 200; left ordinate: grade efficiency against particle size for fill levels U of 20 and 80% at constant rotational speed (n c.) of 40,000 rpm and fill level dependent speed (Δn).

40,000 rpm is significant. Neglecting the consolidation causes a deviation of the predicted batch times of 20%. Although the experimentally observed consolidation at 40,000 rpm was higher, the prediction is in good agreement with the experimental data for all rotational speeds. The experimentally determined separation behavior was published in a previous article.[4] The deviation between predicted and experimentally determined batch time equals 5% at 15,000 rpm and 20% at 40,000 rpm when taking the consolidation into account. By using the validated model, it is possible to calculate the separation of biosuspensions in alternative solid-bowl centrifuge designs and modes of operation, as long as the suspensions are well characterized.

The results presented show a significant dependence of the separation efficiency on the fill level of the centrifuge. If the rotational speed and the throughput are held constant during the batch, the grade efficiency will decrease and, thus, it is not possible to ensure constant particle classification. The loss in residence time due to the sediment build-up can be compensated by increasing the rotational speed, as depicted in Figure 20. The rotational speed compensates for the decreasing residence time and keeps the separation efficiency constant. The dramatic decrease at 2 min is caused by the sedimentation of solids in the acceleration zone of the centrifuge. The sediment growth decreases the thickness of the boundary layer flow as mentioned in the section describing the distribution of the solids. This effect is included in the model presented and has been observed in simulations and experiments.[5,37]

When keeping the rotational speed constant, the grade efficiency $T(x)$ shifts from small particle sizes at a fill level of 20% to coarser particles at a fill level of 80% as shown in Figure 21. If the rotational speed is controlled with the residence time, the overall separation behavior of the centrifuge remains constant and, thus, the grade efficiency curves at both fill levels are congruent to each other. Therefore, the regulation of the rotational speed is suitable to compensate the disadvantage of the semibatch apparatus.

However, the measurement of the fill level during the batch is only feasible by measuring the product loss via, for example, a turbidity sensor. The rotational speed will be increased if the turbidity of the overflow increases. The rotational speed is necessary for keeping the product loss and, thus, the grade efficiency constant are plotted in Figure 20. The maximum rotational speed exceeds 150,000 rpm, which is above the maximum rotational speeds of state-of-the-art tubular-bowl centrifuges. Nevertheless, rotational speed up to 80,000 rpm are feasible with high performance materials for the rotor and magnetic bearings. This leads to a constant process for 87% of the batch time for the example shown in Figure 21.

Conclusions

The model proposed allows the calculation of the sediment build-up in solid-bowl centrifuges, as long as no internal conveying systems are present. The parameters are the rotational speed of the centrifuge, the throughput, solids or volume capacity, the particle-size distribution of the solid phase as well as the properties of the suspension as viscosity and solids volume fraction. The prediction of the consolidation requires the knowledge of the compressive strength and hindered settling function of the sediment (the latter is not necessary for the equilibrium solution). By calculating the volume and mass of the sediment during the semibatch, the process cycle time and efficiency is determined. This model may assist in choosing the most suitable centrifuge for a specific application. The influences of the fill level on the flow pattern are taken into account, which significantly improves the accuracy of the calculated process outcomes with the experimentally measured performance than it would be the case if only the cut size will be calculated. If the sediment influences the residence time, the consolidation of the sediment reduces the influence on the flow pattern and has to be taken into account for fine particulate systems and biological products. The consolidation of the sediment is calculated by applying a 1-D model for discrete elements in the axial direction and integrating over the length of the centrifuge. Taking the consolidation into account improves the accuracy of the prediction when compared with the experimentally observed separation efficiency and sediment build-up. It is possible to calculate the particle-size distribution of the overflow and the sediment and, thus, predict the classifying performance of a centrifuge. Due to the flow pattern and the distribution of the solids throughout the cross-sectional area, the grade efficiency curve exhibits the typical s-shape instead of the theoretical rectangular shape when calculating the cut size of the centrifuge.

The model presented allows the modeling and optimization of process parameters in order to obtain constant separation or classification behavior throughout the duration of the semibatch. Increasing the rotational speed or reducing the throughput compensates for changes in the grade efficiency due to the sediment fill level of the apparatus.

Acknowledgments

The authors would like to thank the Karlsruhe House of Young Scientists (KHYS) and the Particulate Fluids Processing Centre (a Special Research Centre of the Australian Research Council) for funding and support.

Notation

Symbols

A = surface area, m^2
$B(\Phi)$ = dimensionless hindered settling function, –
c = concentration, –
d = width, m
Δl = width of single compartment, m
Δt = timestep, s
L = axial component of settling path, m
L' = reduced length, m
L_0 = length of rotor of centrifuge, m
n = rotational speed, min^{-1}
p^* = pressure scaling, Pa
p_1 = constant of compressive strength function, Pa
p_2 = constant of compressive strength function, –
$p_y(\Phi)$ = compressive strength, Pa s
$P_y(\Phi)$ = dimensionless compressive strength, –
$Q_3(x)$ = cumulative sum size distribution by mass
r = radius, m
$R(\Phi)$ = hindered settling function, Pa s m^{-2}
r_1 = constant of hindered settling function, Pa s m^{-2}
r_2 = constant of hindered settling function, –
t = time, s
T = dimensionless time, –
$T(x)$ = grade efficiency, –
u = solids bulk velocity, m s^{-1}
U = fill level, –
v = axial fluid velocity, m s^{-1}
V = volume, m^3

$\dot{V}$ = volume flux, $m^3\ s^{-1}$
w = settling velocity, $m\ s^{-1}$
W = relative width of the boundary layer, –
x = particle diameter, m
Z = dimensionless height, –
ZC = dimensionless height of sediment, –
ZS = dimensionless height of settling zone, –
$\Delta(\Phi)$ = solids diffusivity, –
$\Delta\rho$ = density difference between solids and liquid, $kg\ m^{-3}$
η = dynamic viscosity, Pa s
τ = residence time, s
Φ = solids concentration in sediment
Ψ = dimensionless solids flux, –
ω = angular velocity, s^{-1}

Indices

0 = initial condition
∞ = infinite solution, equilibrium
bl = boundary layer
boundary = end of boundary layer flow
bowl = bowl of centrifuge
cap = capacity
end = end of simulation
full = capacity of centrifuge reached
g = gel
j = weighted number
pool = surface of the rotating pool in centrifuge
sed = sediment
solids = solids in compartment
Stokes = settling in Stokesian regime
V = volume weighted
weir = weir of centrifuge
xi = volume in feed of Δx

Literature Cited

1. Firth B, Hart G. Size classification in scroll centrifuges. *Int J Coal Prep Util*. 2008;28(3):153–173.
2. Beveridge T. Juice extraction from apples and other fruits and vegetables. *Crit Rev Food Sci Nutr*. 1997;37(5):449–469.
3. Perardi TE, Leffler RAA, Anderson NG. K-series centrifuges II. Performance of the K-II rotor. *Anal Biochem*. 1969;32(3):495–511.
4. Spelter LE, Steiwand A, Nirschl H. Processing of dispersions containing fine particles or biological products in tubular bowl centrifuges. *Chem Eng Sci*. 2010;65(14):4173–4181.
5. Stahl S, Spelter LE, Nirschl H. Investigations on the separation efficiency of tubular bowl centrifuges. *Chem Eng Technol*. 2008;31(11):1577–1583.
6. Buscall R, White LR. The consolidation of concentrated suspensions. 1. The theory of sedimentation. *J Chem Soc Faraday Trans I*. 1987;83:873–891.
7. Landman KA, White LR. Solid/liquid separation of flocculated suspensions. *Adv Colloid Interface Sci*. 1994;51:175–246.
8. Burger R, Karlsen KH. On some upwind difference schemes for the phenomenological sedimentation-consolidation model. *J Eng Math*. 2001;41(2–3):145–166.
9. Stickland AD, White LR, Scales PJ. Modeling of solid-bowl batch centrifugation of flocculated suspensions. *AIChE J*. 2006; 52(4):1351–1362.
10. Barr JD, White LR. Centrifugal drum filtration: I. A compression rheology model of cake formation. *AIChE J*. 2006;52(2):545–556.
11. Barr JD, White LR. Centrifugal drum filtration: II. A compression rheology model of cake draining. *AIChE J*. 2006;52(2):557–564.
12. Bürger R, Concha F. Settling velocities of particulate systems: 12: batch centrifugation of flocculated suspensions. *Int J Miner Process*. 2001;63(3):115–145.
13. Richardson JF, Zaki WN. Sedimentation and fluidisation: part 1. *Chem Eng Res Des*. 1997;75:S82–S99.
14. Bickert G, Stahl W. Settling behavior characterization of submicron particles in dilute and concentrated suspensions. *Part Part Syst Char*. 1997;14(3):142–147.
15. Glinka U. Die Strömung in Überlaufzentrifugen—Neue Ergebnisse mit einem elektrolytischen Markierungsverfahren. *Verfahrenstechnik*. 1983;17(5):315–318.
16. Gösele W. Schichtströmung in Röhrenzentrifugen. *Chemie-Ing. Tech*. 1968;40(13):657–659.
17. Bass E. Strömungen im Fliehkraftfeld I. Periodica Polytechics chem. *Ingenieurwes*. 1959;3:321–340.
18. Bass E. Strömungen im Fliehkraftfeld II—Absetzsicherheit von Röhrenzentrifugen. Periodica Polytechics chem. *Ingenieurwes*. 1959;4:41–61.
19. Leung W. *Industrial Centrifugation Technology*. New York: McGraw-Hill, 1998.
20. Stahl WH. *Industrie-Zentrifugen*. Männedorf: DrM Press, 2004.
21. Spelter LE. *Abtrennung und Klassierung kolloidaler Partikel in Zentrifugen*. Karlsruhe: Cuvillier Verlag, 2012:133.
22. Bass E. Strömungs-und Absetzvorgänge in Röhrenzentrifugen. *Dechema Monographien*. 1962;42:249–264.
23. Horanyi R, Nemeth J. Theoretical investigation of clarification process in a tube centrifuge. *Acta Chim Acad Sci Hung*. 1971;69(1):59–75.
24. Reuter H. Strömungen und Sedimentation in der Überlaufzentrifuge. *Chemie-Ing Tech*. 1967;39(5):311–318.
25. Spelter LE, Nirschl H. Classification of fine particles in high-speed centrifuges. *Chem Eng Technol*. 2010;33(8):1276–1282.
26. Firth B, Hart G. Some aspects of modeling partition curves for size classification. *Int J Coal Prep Util*. 2008;28(3):174–187.
27. Majumder AK, Yerriswamy P, Barnwal JP. The "fish-hook" phenomenon in centrifugal separation of fine particles. *Miner Eng*. 2003;16(10):1005–1007.
28. Schubert H. On the origin of "anomalous" shapes of the separation curve in hydrocyclone separation of fine particles. *Particul Sci Technol*. 2004;22(3):219–234.
29. Nagewararao K. A critical analysis of the fish hook effect in hydrocyclone classifiers. *Chem Eng J*. 2000;80(1–3):251–256.
30. Fernandez XR, Nirschl H. Multiphase CFD simulation of a solid bowl centrifuge. *Chem Eng Technol*. 2009;32(5):719–725.
31. Usher SP, De Kretser RG, Scales PJ. Validation of a new filtration technique for dewaterability characterization. *AIChE J*. 2001;47(7):1561–1570.
32. Erk A. *Rheologische Eigenschaften feindisperser Suspensionen während ihrer Fest-Flüssig-Trennung in Filtern und Zentrifugen*. 1, Herzogenrath: Shaker, 2006.
33. Romani Fernandez X. *Prediction of Multiphase Flow and Separation Efficiency of Industrial Centrifuges by Means of Numerical Simulation*. Karlsruhe: Cuvillier Verlag, 2012.
34. Spelter LE, Schirner J, Nirschl H. A novel approach for determining the flow patterns in centrifuges by means of Laser-Doppler-Anemometry. *Chem Eng Sci*. 2011;66(18):4020–4028.
35. Romani Fernandez X, Nirschl H. A numerical study of the impact of radial baffles in solid bowl centrifuges using computational fluid dynamics. *Phys Sep Sci Eng*. 2010; doi:10.1155/2010/510570.
36. Spelter LE, Meyer K, Nirschl H. Screening of colloids by semi-continuous centrifugation. *Chem Eng Technol*. 2012;35(8):1486–1494.
37. Romani Fernandez X, Spelter LE, Nirschl H. Computational Fluid Dynamics (CFD) and Discrete Element Method (DEM) Applied to Centrifuges, Rijeka: InTech, 2012.

Manuscript received Apr. 12, 2012, and revision received Mar. 8, 2013.